EARTH'S CRYOSPHERE
SCIENTIFIC JOURNAL

Earth's Cryosphere, 2020, vol. XXIV, No. 2, pp. 27–33 **http://earthcryosphere.ru/**

CRYOGENIC PHENOMENA IN SEAS AND OCEANS

DOI: 10.21782/EC2541-9994-2020-2(27-33)

ON THE RELATIONSHIP BETWEEN SEA ICE EXTENT DYNAMICS IN THE NORTHERN HEMISPHERE AND TOTAL ATMOSPHERIC OZONE

V.M. Fedorov, D.M. Frolov

Lomonosov Moscow State University, Faculty of Geography,
1, Leninskie Gory, Moscow, 119991, Russia; fedorov.msu@mail.ru

The sea ice extent dynamics in the Northern Hemisphere and variations of solar irradiance at different altitudes of polar regions are considered as possible controls of total ozone variations in the atmosphere. It has been determined that annual variation of total ozone content (TOC) closely correlates with the annual course and multiyear variations of sea ice extent in the Northern Hemisphere. We used a regression model for forecasting total ozone content up to 2050. It has been revealed that the model concept of total column ozone (TCO) should take into account the Earth's cryosphere effect (cryospheric factor) on variations in total atmospheric ozone. The cryospheric factor includes changes in sea ice extent in the Northern Hemisphere and insolation variations at different altitudes in the polar regions.

Total ozone, sea ice extent, planetary albedo, insolation, insolation contrast, correlation, regression model, forecasting

INTRODUCTION

Due to significance of the ozone layer (acting as a shield to protect Earth's surface from excessive ultraviolet (UV) radiation) to ensure life on Earth (including human), the total atmospheric ozone content (TOC) and its controls is one of the issues of major importance in the Earth Sciences. This provides a substantiation of the topicality of the research into total atmospheric ozone, its spatial and temporal variability.

The TOC studies include two main research directions. The first one is the analysis and advancement of ideas about photochemical reactions leading to production and destruction of ozone (photochemical theory). This research direction is heavily underlain by Chapman's fundamental model (a schematic for photochemical reactions) [*Chapman, 1930*], which principally explains the existence of high-concentration layers of ozone and atomic oxygen in the atmosphere. The second direction focuses on the dynamic aspect [*Perov, Khrgian, 1980*] and includes ideas about atmospheric circulation processes (vortices) and vertical air flows, providing vertical and horizontal transport of ozone between source and sink regions. Our research views the Earth's cryosphere as another element (the third research direction) in the concept of TOC model aiming at studying the seasonal and interannual sea ice extent dynamics largely governed by the change in planetary albedo and water vapor content in polar regions, with particular focus on changes in solar radiation incidence with elevation in polar regions. This paper aims to study the relationships between insolation-affected sea ice extent and TOC at different time scales (annual dynamics, multiyear variability). Variations in albedo correlate with changes in the amount of solar radiation reflected by sea ice into the atmosphere (specifically, 60–90 % by the snow-ice surface and less than 10 % by water surface). Water vapor contents are affected by variations in scattered radiation and concentrations of HO_2 and OH radicals, which contribute to ozone breakup [*Hunt, 1966*]. In addition, changes in sea ice extent may be associated with a good solubility of ozone in water and are thereby involved in the TOC dynamics. As such, this "ice element" is shown to be one of major players in the generalized TOC model because of the maximum TOC values localized in polar regions of the Earth, where the maximum TOC variability (i.e. annual and multiyear variations) is accordingly observed [*Perov, Khrgian, 1980*]. This potential TOC predictor has thus far been totally ignored, though.

Traditionally, ozone is believed to be produced mainly in the equatorial region as a result of photochemical reactions and transported to the polar regions by air masses [*Perov, Khrgian, 1980*]. However, principal features of the solar radiation (insolation) reaching polar regions and production capacity of atmospheric and stratospheric ozone over the poles still remain understudied. Given that during the summer season, polar regions receive more solar radiation

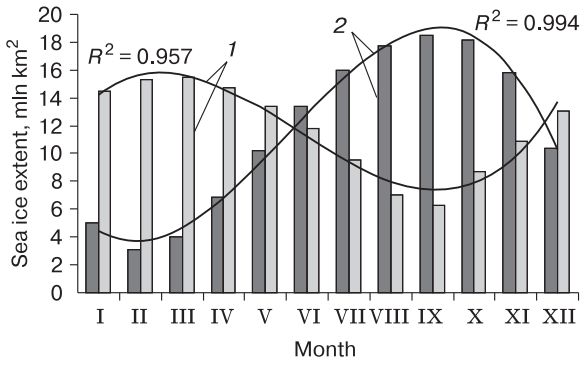

Fig. 1. Seasonal variations in sea ice extent in the Northern (*1*) and Southern (*2*) Hemispheres.

than tropical region (because of the polar day) this period provides at least equal opportunities for ozone production in equatorial region and in polar regions.

The authors' calculations of insolation in different altitude levels [*Fedorov, Kostin, 2019*] show that, e.g. at an altitude of 25 km (an ellipsoid with each point located 25 km above the normal relative to a reference ellipsoid that best approximates the Earth's overall shape) the polar night lasts four months (8–11th astronomical months) in the 84.5–90° latitude range. While in the 84.5–79.5° latitudinal range it lasts two months (9–10th astronomical months), this phenomenon does not occur south of latitude 74.5°. This suggests solar radiation incident for the full year round there and, therefore, a possibility for ozone production. As such, these latitudinal boundaries delimit the surface at 30 km altitude. At an altitude of 35 km, the latitude range of permanent illumination increases by 1° of latitude (75.5°). From a 40 km altitude, the latitude limit of the two-month polar night rises to 84.5° (at an altitude of 25 km, it is located at latitude 79.5°). At altitudes of 45 and 50 km, the latitudinal limit of permanent illumination "builds up" another 1° of latitude (76.5°). As such, the altitude-dependent increase in the latitudinal range of illumination should be taken into account when evaluating a possibility of ozone production in polar regions.

Ice covers about 6 % (ca. 30 million km^2) of the Earth's surface, which is for the most part localized in the Arctic and Antarctic. In the Northern Hemisphere, land ice accounts for only 20 % of the total area of Arctic glaciation, while sea ice for the rest of 80 % [*Koryakin, 1988*]. Seasonal variations in land

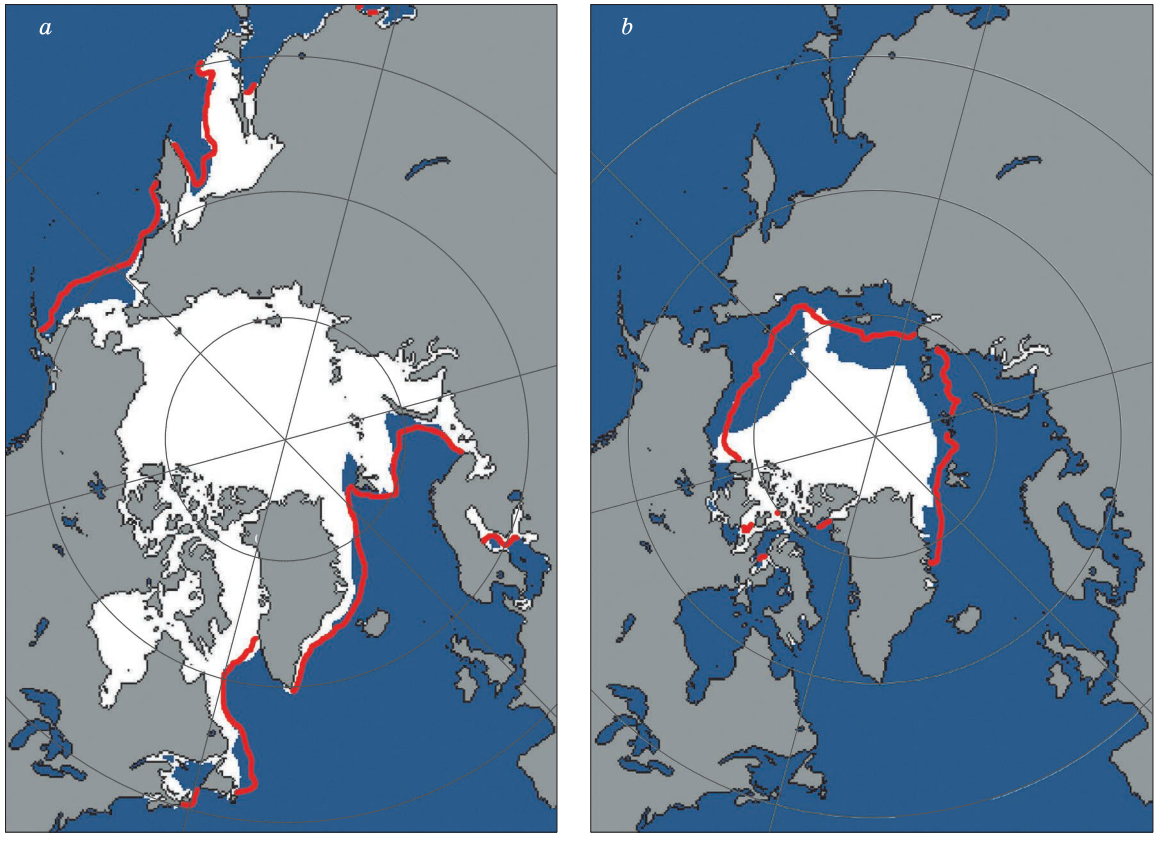

Fig. 2. Changes in sea ice extent in the Northern Hemisphere:

a – March (maximum); *b* – September (minimum). The red line shows the average boundary of sea ice extent in March and November in the period 1981–2010 [*Fetterer et al., 2012;* http://nsidc.org/data/seaice_index/].

and sea glaciation affect the area of 6.3–15.4 million km^2 in the Arctic ocean (Fig. 1) and from 3.0 to 18.5 million km^2 in Antarctica. The amplitude of average seasonal cycle of sea ice area is 9.15 million km^2 in the Northern Hemisphere, and 15.46 million km^2 in the Southern Hemisphere [*Fetterer et al., 2017;* http://nsidc.org]. Seasonal variations in sea ice extent from maximum to minimum (i.e. the amplitude of average seasonal cycle) were estimated (in percentage) for the Northern (59.2 %) and Southern (81.4 %) Hemispheres.

Sea ice cover is a product of interactions between the ocean and the atmosphere under certain temperature conditions [*Frolov, Gavrilo, 1997; Zubakin, 2006*]. The most important parameter is its extent, or the area it occupies. Among the changes this area is subjected to over time, the most pronounced are interpreted as seasonal, interannual and multi-year variations. In the Northern Hemisphere, summer minimum of the sea ice area is chronologically distinctly localized in the annual cycle and falls on September (the autumnal equinox, the end of summer half-year in the Northern Hemisphere) (Fig. 2).

The maximum area is more extended in time and is observed from February through April (the period around vernal equinox, the end of winter and beginning of summer half year in the Northern Hemisphere) [*Frolov, Gavrilo, 1997*]. Accordingly, ultimate sea ice extent values are characterized by ca. 90° phase lag (of three months) in the annual solar irradiance cycle relative to ultimate values of arriving solar radiation.

RESULTS AND DISCUSSION

The relationships between TOC values and sea ice extent (SIE) in the Northern hemisphere were analyzed with respect to annual variation cycles and time-series of multiyear variability. The input data for seasonal TOC variations were combined with the SBUV satellite database (Version 8.6) Merged Ozone Data Set (MOD) 1970–2017 Profile and Total Column Ozone from the SBUV Instrument Series [https://acd-ext.gsfc.nasa.gov/Data_services/merged/]. These data include TOC values with a monthly resolution and in 5° increments of latitude spanning the period since 1970 to the present.

The applied herewith measures of TOC are related to the concept of the total column ozone (TCO) and use units of length (centimeters, millimeters, and micrometers). The total column ozone implies total ozone content in a vertical air column conceptualized by suggesting that all of the overhead ozone molecules (spread over the stratosphere thickness) could be brought down to form a "layer" at standard conditions (pressure p = 1013 mbar, temperature T = 273.16 K). Thus, the units used as measures of the ozone column base ("thickness") are as follows: atmosphere-centimeters (atm-cm) and milliatmospheric centimeters (matm-cm), which alternatively are termed Dobson Units (DU) [*Perov, Khrgian, 1980*]. According to the Mid-Latitude Ozone Model [*Krueger, Minzner, 1976*], the "thickness " of TCO layer is 0.345 atm-cm (or 345 DU). This value is equivalent to ozone concentration in $7.39 \cdot 10^{-3}$ kg, or $9.27 \cdot 10^{22}$ molecules contained in a column of air with a 1 m^2 cross-sectional area (i.e. for every square meter of area at the base of the column) [*Perov, Khrgian, 1980*]. In this work, we use Dobson Units (DU) for the atmospheric TOC analysis. The initial data on the sea ice extent were derived from satellite observations available on the US National data center website [http://nsidc.org].

Annual TOC variation cycle

The annual TOC variations cycle ("annual course") is characterized by the antiphase change in the hemispheres (Fig. 3).

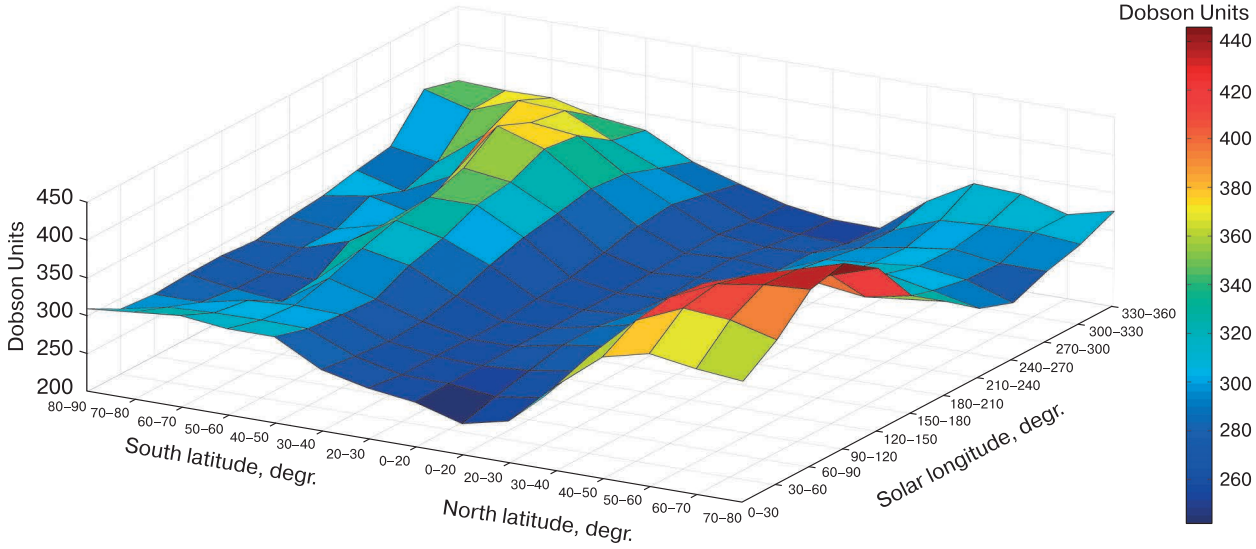

Fig. 3. Planetary total ozone distribution and ist changes with seasons and latitudes.

In the Northern Hemisphere, the maximum TOC values are reported in April, and minimum in October, whereas in the Southern Hemisphere, vice versa, the minima in TOC values are attributable to April, and maxima to October. That same antiphase dynamics is observed in the annual SIE retreat/advance cycles in the hemispheres. In the Northern Hemisphere, SIE values peak in March, and are the lowest in September (in the Southern Hemisphere, contrarywise). Thus, the TOC maxima and minima are immediately followed by SIE maxima and minima. The effect is offset by lag of about a month. The shift by a month ahead in annual TOC variations (if its annual variation cycle is synchronized with the SIE annual dynamics) the coefficient of correlation between the time-series equals 0.974 (with probability of 0.99) (Fig. 4). The statistical significance of the linear correlation coefficient was evaluated from the correlation analysis according to the existing evaluation criteria and methods [*Tsymbalenko et al., 2007*].

The annual TOC variation cycle for the Earth is determined by annual cycle of TOC variations in the Northern Hemisphere (and its anti-phase in the Southern Hemisphere, accordingly). This owes to greater TOC values for the Northern Hemisphere against the Southern Hemisphere. The mean monthly TOC values are 325.26 DU for the Northern Hemisphere and 302.95 DU for the Southern Hemisphere [*Perov, Khrgian, 1980*]. If compared, these are expressed as percentage showing that mean monthly TOC values the Northern Hemisphere are ca. 7 % less than those for Northern Hemisphere. Interestingly, during winter half year in the two hemispheres, the Northern Hemisphere receives about 7 % more solar radiation than the Southern Hemisphere [*Fedorov, 2018*]. This phenomenon accounts for the fact that during winter half year in the Northern Hemisphere, the Earth reaches perihelion, while it reaches aphelion in winter half year in the Southern Hemisphere. In summer half year, the effect is therefore seen to be opposite (i.e. roughly 6 months apart). Given that during the winter half year in the two hemispheres, Northern Hemisphere receives more solar radiation versus Southern Hemisphere, the former sees more reflected and scattered radiation due to the maximum sea ice extent at this time of year. This may also be one of the reasons for asymmetry in the TOC distributions across the hemispheres.

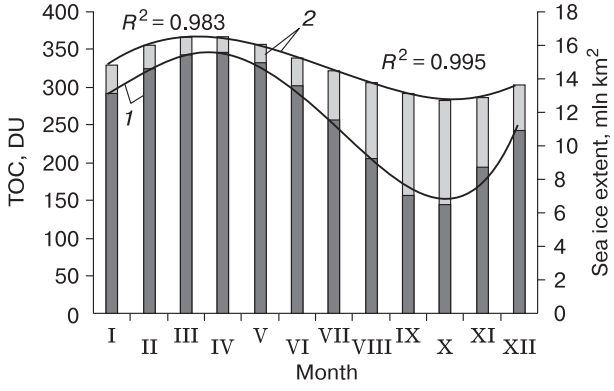

Fig. 4. Seasonal variation cycle of sea ice extent in the Northern Hemisphere (*1*) and TOC (*2*).

TOC time-series is one month phase-shifted (advanced).

Hemispheric asymmetry in total ozone distribution can be dealt with by the dynamic approach, which constitutes the dynamic element of the TOC model, to study the global atmospheric circulation pattern in the hemispheres and specific characteristics of the insolation because of elliptical orbit of the Earth and ozone production in winter months at high altitudes in the polar regions. The TOC models are a whole family of models, and each presents parameterization of dynamic factors and photochemical processes in a different way. Meridional ozone transport in the Northern Hemisphere occurs both by regular transport in the global atmospheric circulation (GAC) with its constituent wind cells – Hadley Cells, Ferrell Cells, Polar Cells, and vortexes (tropical and extratropical cyclones) [*Perov, Khrgian, 1980; Fedorov, 2018*]. Due to the greater heterogeneity of the underlying surface in the Northern Hemisphere, meridional ozone transport is carried out there by tropical and extratropical cyclones (to a far greater extent than in the relatively homogeneous Southern Hemisphere). In addition, as it was shown previously [*Fedorov, 2018*], an increase in the meridional transport intensity (meridional insolation gradient) is observed in winter half year in the Polar Cells, while it decreases in summer half year. An increase in the annual meridional insolation gradient (heat transfer) is observed in the areas of localization of the Hadley and Ferrell circulation cells. The ratio of land to ocean area is important as descriptor of the heterogeneity of the underlying surface in the hemispheres. The proportions of land/ocean areas are: 39.3 % and 60.7 % in the Northern Hemisphere and 19.1 % and 80.9 % in the Southern Hemisphere, respectively [*Istoshin, 1956*]. Thus, the annual number of tropical cyclones in the Northern Hemisphere (North Atlantic and North-Western Pacific) totals to about 60 on average, and considerably less (6–8) in the Southern Hemisphere [http://meteoinfo.ru]. In the Southern Hemisphere, the meridional ozone transport is blocked due to the strong Roaring Forties west-east transport, whose existence is associated with the uniformity of the hemisphere and a high meridional temperature gradient (much higher than the meridional temperature gradient in the Northern Hemisphere). Specifically, these natural controls, which weaken the meridional ozone transport effect in the Southern Hemisphere, are likely to determine the TOC values asymmetry for the two hemispheres.

The physical mechanism of the maximum and minimum TOC distribution can be qualitatively represented as follows. Since the beginning of the vernal equinox (March–April), the illuminated area in the Northern Hemisphere extends north of the Arctic circle (66.6°). While the solar declination is small, and is associated with large amount of the scattered radiation. At this, sea ice extent approaches its maximum, thereby increasing the reflected radiation. These components of the incoming radiation are likely to determine both production and peaks in TOC in the Northern Hemisphere (which also occurs in the Southern Hemisphere after the onset of autumnal equinox in the Northern Hemisphere). The time of approaching autumnal equinox is marked by a small solar declination in the Northern Hemisphere; lowest the sea ice spread; and minimal reflected radiation, which probably determines the minimum TOC values (the Southern Hemisphere sees the same situation with the onset of spring in the Northern Hemisphere). In addition, the atmospheric circulation polar cells show an increase in intensity in winter half year [*Fedorov, 2018*], which means that the maximum observed after the vernal equinox may also be associated with this dynamic factor.

Mutiyear variations in TOC

The authors compared the multiyear changes in the average annual TOC values obtained from the observations over the period 1936–2016 at Arosa station (Switzerland) [https://www.woudc.org/], with the SIE values derived from the reconstructions for the period from 1936 to 2006 [*Walsh, Chapman, 2001*] and using a regression model from 2007 to 2016 [*Fedorov, 2015a; Fedorov, Grebennikov, 2018*]. This time-series of TOC measurements is the longest [*Bronnimann et al., 2000; Visheratin, 2007; Staehelin et al., 2018*].

Implementation of the cryosphere modulus (sea ice extent in the Northern Hemisphere) in our studies of multiyear variations in the atmospheric TOC is determined by the reasons discussed above. Firstly, the annual TOC variation cycle in the atmosphere is determined by the annual TOC variations in the atmosphere of the Northern Hemisphere. Secondly, there are no long series of observations of sea ice area in the Southern Hemisphere (except relatively short satellite observation series since 1978). Results of the comparison showed a close correlation between the series of multiyear TOC variations and multiyear SIE dynamics in the Northern Hemisphere. The correlation coefficient (R) for multiyear TOC variations and multiyear average annual SIE in the Northern Hemisphere is 0.671. A relationship between multiyear TOC variations with the minimum sea ice extent is characterized by the value $R = 0.642$. The ties with the maximum values for sea ice extent dynamics are slightly weaker ($R = 0.558$). All R values are statistically significant with a probability (p-value) of 0.99. When smoothing the TOC and SIE time-series and using the method of five-year smoothed moving averages, the R values accordingly become equal to 0.899, 0.859, and 0.857 (Fig. 5).

Previously, the authors calculated the solar radiation that arrives at the top (upper boundary) of the atmosphere with a large spatial and temporal resolution [*Fedorov, 2015b, 2019; Fedorov, Frolov, 2019*]. The calculations of the incoming solar radiation were performed using the data obtained from high-precision astronomical ephemerides [*Giorgini et al., 1996*; http://ssd.jpl.nasa.gov] for the entire Earth's surface (no atmosphere) within the interval from 3000 BC to 2999 AD. The input astronomical data for calculating insolation were the declination and ecliptic longitude of the Sun, the distance from the Earth to the Sun, and difference between the course of uniformly running (coordinate time, CT) and the universal corrected time (universal time, UT). The surface of the Earth was approximated by ellipsoid (GRS80–Geodetic Reference System 1980) with semi-axis lengths 6,378,137 m (big one) and 6,356,752 m (small one). The calculation algorithm can be generally represented by the expression

$$I_{nm}(\varphi_1,\varphi_2)=\int_{t_1}^{t_2}\left(\int_{\varphi_1}^{\varphi_2}\sigma(H,\varphi)\left(\int_{-\pi}^{\pi}\Lambda(H,t,\varphi,\alpha)\,d\alpha\right)d\varphi\right)dt,$$

where I is the incoming solar radiation for the elementary n-th fragment of the m-th of the tropical year, J; σ is the square multiplier, m^2, which enables calculation of the square differential $\sigma(H,\varphi)$; $d\alpha d\varphi$ is the square of infinitely small trapezoid ellipsoid cells; α is horary angle, rad unit; φ is geographical latitude, rad unit; H is the height of the ellipsoid surface relative to Earth surface, m; $\Lambda(H,t,\varphi,\alpha)$ is insolation at the stated moment at the stated ellipsoid surface point, W/m^2; t is time, s. The integration steps were: longitude 1°, latitude 1°, defined as one three hundred sixtieth (1/360) of the length of tropical year [*Fedorov, 2013*]. The value of solar constant (average multiyear TSI value (total solar irradiance)) was taken to be 1361 W/m^2 [*Kopp, Lean, 2011*]. Changes in the solar activity were not taken into consideration [*Fedorov, 2015b, 2019; Fedorov, Kostin, 2019; Fedorov, Frolov, 2019*].

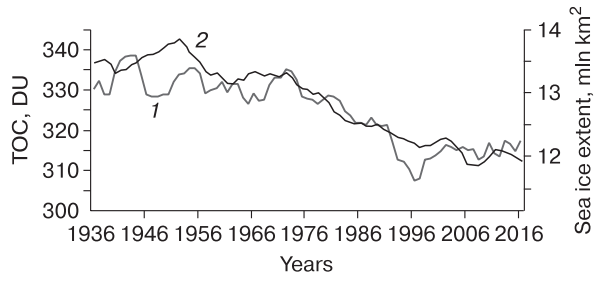

Fig. 5. The five-year-period smoothed moving averages of TOC time-series (*1*) and average annual sea ice extent in the Northern Hemisphere (*2*).

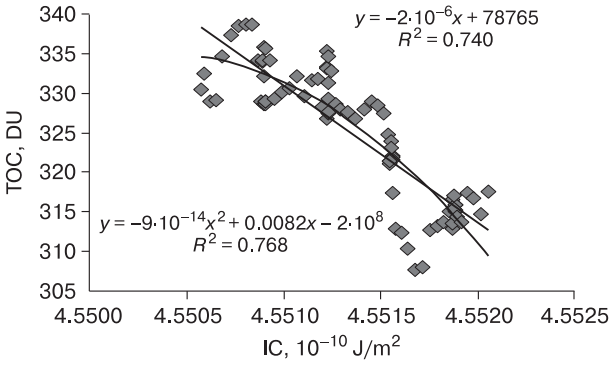

Fig. 6. Graphs of linear and polynomial (second-degree) regressions for IC and TOC and equations.

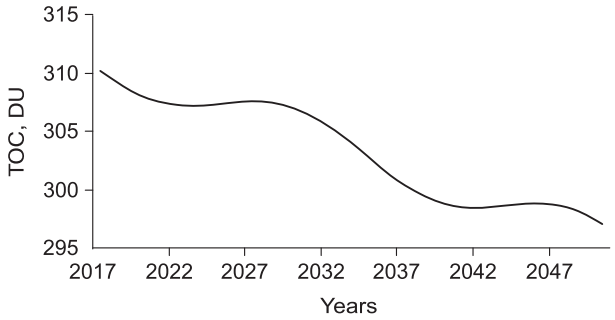

Fig. 8. Forecast estimations of TOC variations calculated based on the ensemble of linear and polynomial (second-degree) regression model.

A close relationship was revealed between multiyear changes in the insolation (irradiance) contrast (IC) and multiyear variations in sea ice extent in the Northern hemisphere [*Fedorov, 2015a; Fedorov, Grebennikov, 2018*]. The authors interpret IC as the difference between annual insolation of the heat source area (0–45° latitude) and heat sink area (45–90° latitude) in the two hemispheres. IC (for heat source and sink areas) generally reflects changes in the meridional gradient of insolation, which controls meridional heat transfer in the ocean–atmosphere system [*Fedorov, 2018, 2019*]. In the regression equations, multiyear changes in IC explain 76 % of the multiyear variability of the average annual and minimum SIE in the Northern Hemisphere [*Fedorov, Grebennikov, 2018*]. A relationship between TOC and IC time-series is characterized by the value $R = -0.657$ (with a probability of 0.99), while the smoothed (for five-year moving averages) TOC time-series – by the value $R = -0.860$. The IC is extrapolated by the authors onto the future, allow to perform an estimated forecast of smoothed TOC values (trends) based on a regression model. Graphs of the linear and polynomial (second-degree polynomial) regression equation are shown in Fig. 6. The coefficient of determination (R^2) shows the proportion of multiyear variability of TOC, which is taken into account by the regression model (IC).

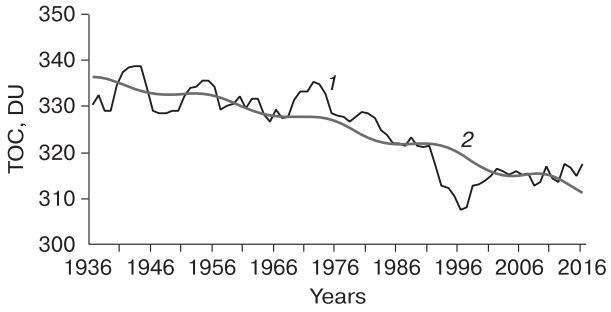

Fig. 7. Measured (*1*) and calculated from ensemble (*2*) TOC values.

TOC calculations were performed using linear and polynomial regression equations. In these equations, a 74.0 % and 76.8 % change in TOC is determined by a variation in IC. The average regression model based on an ensemble of linear and polynomial solutions revealed that as much as 76.1 % of the multiyear variability of TOC is determined by multiyear changes in the IC (or the average annual and minimum SIE) (Fig. 7).

The estimated forecast is calculated for the TOC values smoothed over a five-year moving averages (TOC trends). According to the calculations, the TOC in 2050 will be 297 DU (Fig. 8). The reduction in total ozone will be 14 DU, against the values as of 2016. Thus, the TOC reduction in 2050 relative to 2016 will be 4.5 %. The probable reasons for atmospheric ozone reduction are: reduction in the sea ice extent (primarily in the Northern Hemisphere) and affiliated decrease in the planetary albedo; and a marked decrease in the amount of solar radiation reaching the polar regions [*Fedorov, 2015b, 2018*].

CONCLUSION

The sea ice extent dynamics and insolation interpreted to be as factors of seasonal and multiyear TOC variations are considered. Characteristic features of spatial and temporal sea ice extent dynamics, insolation and TOC variations are revealed. It was determined that the annual and multiyear TOC variations are closely related to annual and multiyear variations in sea ice extent in the Northern Hemisphere (correlation coefficient is 0.974 for the annual variation cycle and from 0.857 to 0.899 for multiyear variations). The annual sea ice extent dynamics is strongly correlated with the annual dynamics of insolation, while multiyear sea ice extent variations – with multiyear IC variations [*Fedorov, 2015a*]. Based on the calculated IC values, smoothed TOC values enabled estimation of the forecast values for the period up to 2050. It is shown that in the model conceptualization

of TOC, next to the photochemical reactions and dynamic (variations) modules, the Earth's cryosphere should be considered as a factor affecting TOC variations, which also implicated in the sea ice extent dynamics in the Northern Hemisphere and altitude-specific changes in insolation in the polar regions.

The work was carried out within the state-commissioned budget theme "Geoecological analysis and forecast of the permafrost dynamics in the Russian Arctic" (AAAA-A16-116032810055-0) and "Mapping, modeling and risk evakuation of natural hazards" (AAAA-A16-116032810093-2).

References

Bronnimann, S., Luterbacher, J., Schmutz, C., Wanner, H., 2000. Variability of total ozone Aroza, Switzerland, since 1931 related to atmospheric circulation indices. Geophys. Res. Lett. 27 (15), 2213–2216.

Chapman, S., 1930. On ozone and atomic oxygen in the upper atmosphere. Phil. Mag. Ser. 7, vol. 10 (64), 369–385.

Fedorov, V.M., 2013. Interannual variations in the duration of the tropical year. Doklady Earth Sciences 451, pt. 1, 750–753, DOI: 10.1134/S1028334X13070015.

Fedorov, V.M., 2015a. Trends of the changes in sea ice extent in the Northern Hemisphere and their causes. Earth's Cryosphere XIX (3), 46–57.

Fedorov, V.M., 2015b. Spatial and temporal variation in solar climate of the Earth in the present epoch. Geophys. Processes and Biosphere 14 (1), 5–22.

Fedorov, V.M., 2018. The Earth's Insolation and Current Climate Changes. Fizmatlit, Moscow, 232 pp. (in Russian).

Fedorov, V.M., 2019. Earth insolation variation and its incorporation into physical and mathematical climate models. Physics Uspekhi 62 (1), 32–45, DOI: 10.3367/UFNe.2017.12.038267.

Fedorov, V.M., Frolov, D.M., 2019. Spatial and temporal variability of solar radiation arriving at the top the atmosphere. Cosmic Research (English translation of kosimicheskie issledovaniya), Maik Nauka/Interperiodica Publishing (Russian Federation), vol. 57 (3), 156–162, DOI: 10.1134/S0010952519030043.

Fedorov, V.M., Grebennikov, P.B., 2018. Insolation contrast of the Earth and changes in the sea ice extent in the Northern Hemisphere. The Arctic: Ecology and Economy, No. 4 (32), 86–94.

Fedorov, V.M., Kostin, A.A., 2019. Insolation calculations for the period from 3000 BC to 2999 AD. Protsessy v geosredakh (Processes in Geoenvironments), No. 2, 254–262.

Fetterer, F., Knowles, K., Meier, W., et al., 2017. Updated daily sea ice index, version 3. Boulder, Colorado USA. NSIDC: National Snow and Ice Data Center, DOI: 10.7265/N5K072F8.

Frolov, I.E., Gavrilo, V.P. (Eds.), 1997. Sea Ice. Gidrometeoizdat, St. Petersburg, 402 pp. (in Russian).

Giorgini, J.D., Yeomans, D.K., Chamberlin, A.B., et al., 1996. JPL's On-Line Solar System Data Service. Bull. Amer. Astronomical Soc. 28 (3), 1158.

Hunt, B.G., 1966. The need for a modified photochemical theory of the ozonosphere. J. Atmos. Sci. 23 (1), 88–95.

Istoshin, Yu.V., 1956. The Oceanography. Gidrometeoizdat, Leningrad, 304 pp. (in Russian).

Kopp, G., Lean, J., 2011. A new lower value of total solar irradiance: Evidence and climate significance. Geophys. Res. Lett. 37, p. L01706, DOI: 10.1029/2010GL045777.

Koryakin, V.S., 1988. Arctic Glaciers. Nauka, Moscow, 160 pp. (in Russian).

Krueger, A.J., Minzner, R.A., 1976. A mid-latitude ozone model for the 1976 U.S. Standard Atmosphere. J. Geophys. Res. 81 (24), 4477–4481.

Perov, S.P., Khrgian, F.Kh., 1980. Modern Atmospheric Ozone Problems. Gidrometeoizdat, Leningrad, 288 pp. (in Russian)

Staehelin, J., Renaud, A., Bader, J., et al., 1998. Total ozone series at Arosa (Switzerland): Homogenization and data comparison. J. Geophys. Res. 103, No. DS, 5827–5841, DOI: 10.1029/97JD02402.

Staehelin, J., Viatte, P., Stubi, R., et al., 2018. Stratospheric ozone measurements at Aroza (Switzerland): history and scientific relevance. Anmos. Chem. Phys. 18, 6567–6584, DOI: 10.5194/acp-18-6567-2018.

Tsymbalenko, T.T., Baydakov, A.N., Tsimbalenko, O.S., Gladilin, A.V., 2007. Methods of Mathematical Statistics in the Processing of Economic Information. Finansy i Statistika, Moscow, 200 pp. (in Russian).

Visheratin, K.N., 2007. Interannual variations and trends in zonal mean series of total ozone, temperature and zonal wind. Izv. RAS. FAO, 43 (4), 67–85.

Walsh, J.T., Chapman, W.L., 2001. 20th century sea-ice variations from observational data. Ann. Glaciol. 33, 444–448.

Zubakin, G.K. (Ed.), 2006. Ice Formations in the Western Arctic Seas. AANII, St. Petersburg, 272 pp. (in Russian).

URL: http://nsidc.org/ (last visited: 25.08.2019).

URL: https://acd-ext.gsfc.nasa.gov/Data_services/merged/ (last visited: 25.08.2019).

URL: http://meteoinfo.ru/ (last visited: 25.08.2019).

URL: https://www.woudc.org/ (last visited: 25.08.2019).

URL: http://ssd.jpl.nasa.gov/ – NASA, Jet Propulsion Laboratory California Institute of Technology (JPL Solar System Dynamics) (last visited: 25.08.2019).

Received August 30, 2019
Revised version received November 6, 2019
Accepted December 3, 2019